

Alfvén Wave Mode Conversion in Neutron Star Magnetospheres: A Semi-analytic Approach

ALEXANDER Y. CHEN,¹ YAJIE YUAN,¹ AND DOMINIC BERNARDI¹

¹*Physics Department and McDonnell Center for the Space Sciences, Washington University in St. Louis, MO, 63130, USA*

ABSTRACT

We write down the force-free electrodynamics (FFE) equations in dipole coordinates, and solve for normal modes corresponding to Alfvénic perturbations in the magnetosphere of a neutron star. We show that a single Alfvén wave propagating on dipole field lines spontaneously sources a fast magnetosonic (fms) wave at the next order in the perturbation expansion, without needing 3-wave interaction. The frequency of the sourced fms wave is twice the original Alfvén wave frequency, and the wave propagates spherically outwards. The properties of the outgoing fms wave can be computed exactly using the usual devices of classical electrodynamics. We extend the calculation to the closed zone of a rotating neutron star magnetosphere, and show that the Alfvén wave also sources a spherical fms wave but at the same frequency as the primary Alfvén wave.

Keywords: magnetic fields — stars: neutron — plasma astrophysics — Alfvén waves — perturbation theory

1. INTRODUCTION

Nonlinear wave phenomena in the magnetospheres of neutron stars have recently garnered significant attention in the community. It was demonstrated through first-principles force-free simulations that small-amplitude Alfvén waves can spontaneously convert to fast magnetosonic (fms) waves (Yuan et al. 2021), and large-amplitude Alfvén waves can become nonlinear and break the background magnetic field lines, launching a relativistic ejecta (Yuan et al. 2020, 2022). This relativistic ejecta can potentially launch shocks at large radii and power Fast Ra-

dio Bursts (FRBs) (e.g. Metzger et al. 2019; Plotnikov & Sironi 2019; Sironi et al. 2021). Alfvén waves propagating on curved magnetic field lines also suffer from transverse steepening (also called dephasing by Bransgrove et al. (2020)), which leads to spontaneous increase in k_{\perp} as the wave propagates and may lead to charge separation (Chen et al. 2022a).

In addition, recent simulations also studied nonlinear interactions between colliding Alfvén waves. For oppositely polarized Alfvén waves, their magnetic field components may cancel, leaving a region with $E > B$ (Li et al. 2019, 2021). This can lead to fast dissipation of the colliding Alfvén wave, creating an evanescent current sheet that can give rise to non-thermal particle acceleration. TenBarge et al.

(2021) and Nättilä & Beloborodov (2022) studied the collision between two oblique relativistic Alfvén waves, and found that this process generally leads to a turbulent cascade. In particular, Nättilä & Beloborodov (2022) showed that charge-starvation may occur during such a cascade which leads to a distinct dissipation mechanism.

Fast magnetosonic waves, on the other hand, can steepen into very strong shocks when they become nonlinear (Chen et al. 2022b; Beloborodov 2023a). This mechanism can in principle provide strong constraints on the location where FRBs are produced, preventing FRBs emitted near the star to escape from the closed zone of the magnetosphere (Beloborodov 2023b). Even in regimes where the fms wave does not steepen, it may still suffer from significantly enhanced scattering cross section with charge particles, leading to strong energy loss and limiting the optically thin region to a small cone near the magnetic axis (Beloborodov 2022; Qu et al. 2022). Pulses of fms waves can interact with the equatorial current sheet near the light cylinder, leading to fast reconnection that can also potentially produce FRB signals (Lyubarsky 2020; Mahlmann et al. 2022; Wang et al. 2023). The fms waves may spontaneously decay into Alfvén waves through 3-wave interaction and their energy transferred to small scales directly (Golbraikh & Lyubarsky 2023). It was also recently proposed that fms waves may also scatter off magnetospheric plasma via inverse Compton scattering, which can be another potential channel for producing FRB signals from within the magnetosphere (Qu et al. in prep.).

The nonlinear phenomena associated with Alfvén waves and fms waves are often analyzed in the WKB framework, where the wavelength is taken to be much smaller than the global length scale L (e.g. the length of the magnetic field line on which they propagate) (Brans-

grove et al. 2020; Yuan et al. 2021; Golbraikh & Lyubarsky 2023). Similarly, in many of the simulation works on wave interactions cited above, the curvature of the background magnetic field is often ignored. However, for Alfvén waves launched by star quakes, their characteristic angular frequency can be ~ 10 kHz (e.g. Bransgrove et al. 2020), leading to a macroscopic wavelength $\lambda_A \sim 3 \times 10^6$ cm. As a result, the WKB assumption of $kL \gg 1$ may not always be reasonable especially for field lines close to the star.

We believe a solution of the Alfvén wave in a dipole background magnetic field can help facilitate the study of various nonlinear phenomena in the neutron star magnetosphere. To our knowledge, such a solution does not explicitly exist in the literature, and it can potentially be used to elucidate the nature of nonlinear wave mode conversion in the magnetosphere. In this work, we attempt to construct such a solution under an asymptotic expansion in wave amplitude, without resorting to a WKB approximation. Then, we study the higher order effects caused by the propagation of this Alfvén wave. In particular, we focus on its conversion into fms waves within the neutron star magnetosphere.

This paper is organized into three main parts. In Section 2, we derive the equation governing Alfvénic normal modes in dipole geometry. We solve the equation numerically and compare it with previously suggested approximate results. In Section 3, we expand the field quantities to second order and show that the primary Alfvén wave spontaneously sources a second-order fms wave due to the geometry of dipole field lines. We use the numerical solution from Section 2 to compute the conversion rate to fms waves and discuss parameter scaling. In Section 4, we carry out a two-scale asymptotic expansion in both electromagnetic perturbation amplitude and rotation velocity. We show that a similar conversion to fms waves now happens at first

order in both perturbation amplitude and rotation. Finally in Section 5 we discuss potential implications of this work and future directions.

2. ALFVÉN WAVES IN A NON-ROTATING DIPOLE MAGNETOSPHERE

In a dipole background magnetic field, the magnetic flux coordinates align with the dipole field lines. There are multiple ways to construct an orthogonal coordinate system out of this geometry (e.g. [Kageyama et al. 2006](#)), but we will adopt the standard dipole coordinates for this paper:

$$q = \frac{\cos \theta}{r^2}, \quad p = \frac{r}{\sin^2 \theta}, \quad \phi = \phi, \quad (1)$$

where q varies along the dipole field line, and p varies perpendicular to the field line. Note that q increases from the southern hemisphere to the northern hemisphere due to the factor of $\cos \theta$. The variable p labels individual field lines and marks their maximum extent, $p = r_{\max}$. We also define an auxiliary quantity $\delta = \sqrt{1 + 3 \cos^2 \theta}$. A number of useful expressions including vector calculus identities are listed in Appendix A.

The force-free equations read (see e.g. [Gruzinov 1999](#)):

$$\begin{aligned} \partial_t \mathbf{E} &= c \nabla \times \mathbf{B} - 4\pi \mathbf{j} \\ \partial_t \mathbf{B} &= -c \nabla \times \mathbf{E} \\ \mathbf{j} &= \frac{c}{4\pi} \frac{\mathbf{B} \cdot \nabla \times \mathbf{B} - \mathbf{E} \cdot \nabla \times \mathbf{E}}{B^2} \mathbf{B} \\ &\quad + \frac{c}{4\pi} \nabla \cdot \mathbf{E} \frac{\mathbf{E} \times \mathbf{B}}{B^2}. \end{aligned} \quad (2)$$

We decompose the electromagnetic fields in an asymptotic expansion in $\delta B/B_0$ where B_0 is the strength of the background magnetic field:

$$\begin{aligned} \mathbf{B} &= \mathbf{B}^{(0)} + \mathbf{B}^{(1)} + \mathbf{B}^{(2)} + \dots \\ \mathbf{E} &= \mathbf{E}^{(0)} + \mathbf{E}^{(1)} + \mathbf{E}^{(2)} + \dots \end{aligned} \quad (3)$$

where $\mathbf{B}^{(0)} = \mathbf{B}_0 \propto r^{-3} \hat{\mathbf{q}}$ is the dipole background, and $\mathbf{E}^{(0)} = 0$. We seek wave solutions for the first order fields $\mathbf{E}^{(1)}$ and $\mathbf{B}^{(1)}$.

In axisymmetry, Alfvén waves have magnetic perturbation in the $\hat{\phi}$ direction. They are ducted along the field line, and their amplitude scales as approximately $r^{-3/2}$. Therefore, we look for 2D solutions of the following general form:

$$\mathbf{B}^{(1)} = r^{-3/2} e^{-i\omega t} f(p, q) \hat{\phi}. \quad (4)$$

and our goal is to determine the unknown function $f(p, q)$. This is equivalent to taking a Fourier transform in time on the linearized equations, and we are seeking the normal modes of electromagnetic oscillations in the dipole geometry. [Chen et al. \(2022a\)](#) wrote down an ansatz for the Alfvén wave solution that is equivalent to $f(p, q) = \exp(\Phi_0(p) + ik_{\parallel} s)$ where s is the field line length measured from the launching footpoint, and Φ_0 is the initial wave phase that may be different on different field lines. In the following, we will derive the equation governing $f(p, q)$ and check whether this ansatz is correct.

The first order force-free current density is given by only a single term since the background $\mathbf{E}^{(0)}$ vanishes and $\nabla \times \mathbf{B}^{(0)} = 0$:

$$\mathbf{j}^{(1)} = \frac{c}{4\pi} \frac{\mathbf{B}^{(0)} \cdot \nabla \times \mathbf{B}^{(1)}}{B_0^2} \mathbf{B}^{(0)}. \quad (5)$$

Plugging the Alfvén wave ansatz and this first order current into the Maxwell equations, it can be seen that $\mathbf{j}^{(1)}$ cancels the $\hat{\mathbf{q}}$ component of $\nabla \times \mathbf{B}^{(1)}$, leaving only $\hat{\mathbf{p}}$ component for $\partial \mathbf{E}^{(1)}/\partial t$:

$$\begin{aligned} \partial_t \mathbf{E}^{(1)} &= c \nabla \times \mathbf{B}^{(1)} - 4\pi \mathbf{j}^{(1)} \\ &= c \hat{\mathbf{p}} \left[-\frac{\delta}{r^3} \frac{\partial B_{\phi}^{(1)}}{\partial q} + \frac{3 \cos \theta}{r \delta} B_{\phi}^{(1)} \right] \\ &= c \hat{\mathbf{p}} \left(-\frac{\delta}{r^3} \frac{\partial_q f}{f} B_{\phi}^{(1)} \right). \end{aligned} \quad (6)$$

The factor of $r^{-3/2}$ in Equation (4) leads to a cancellation of the second term on the second line, resulting in a relatively simple expression. If we assume $e^{-i\omega t}$ time dependence for $\mathbf{E}^{(1)}$ as

well, then:

$$E_p^{(1)} = -\frac{ic}{\omega} \frac{\delta}{r^3} \frac{\partial_q f}{f} B_\phi^{(1)}. \quad (7)$$

Given that \mathbf{E} is only nonzero in the $\hat{\mathbf{p}}$ direction, the other Maxwell equation can be simplified too:

$$\begin{aligned} \partial_t \mathbf{B}^{(1)} &= -c \nabla \times \mathbf{E}^{(1)} \\ &= -c \hat{\phi} \left[\frac{\delta}{r^3} \frac{\partial E_p^{(1)}}{\partial q} - \frac{6 \cos \theta}{r \delta^3} (1 + \cos^2 \theta) E_p^{(1)} \right] \end{aligned} \quad (8)$$

Combining Equations (6) and (8), we can write down a second-order differential equation for the unknown function $f(p, q)$:

$$\partial_q (r^{-3} \partial_q f) = -\left(\frac{\omega}{c}\right)^2 \frac{r^6}{\delta^2} f. \quad (9)$$

In particular, $f \propto e^{ik_{\parallel}s}$ turns out not to be a solution to Equation (9). Plugging it in and using $\partial s / \partial q = r^3 / \delta$, we are left with $ik_{\parallel} f \partial_q (1/\delta) = 0$, which does not hold for general k_{\parallel} .

Note that Equation (9) has no p derivatives, which means that the wave profile is essentially decoupled between field lines. The wave on each field line propagates independently. Bransgrove et al. (2020) also explicitly used this property when evolving the Alfvén waves in the magnetosphere. We can therefore specialize to a single magnetic field line with constant p , i.e. $r = p \sin^2 \theta$, and interpret the equation as an ODE. It is also possible to change the variable from q to $\mu = \cos \theta$ to further simplify the equation:

$$\frac{d}{d\mu} \left(\frac{1}{1 + 3\mu^2} \frac{df}{d\mu} \right) = -\kappa^2 f, \quad (10)$$

where we have defined a dimensionless wave number $\kappa = \omega p / c$ that can be understood as the ratio between p and the Alfvén wavelength λ . This is the differential equation governing the spatial part of Alfvén waves in dipole geometry.

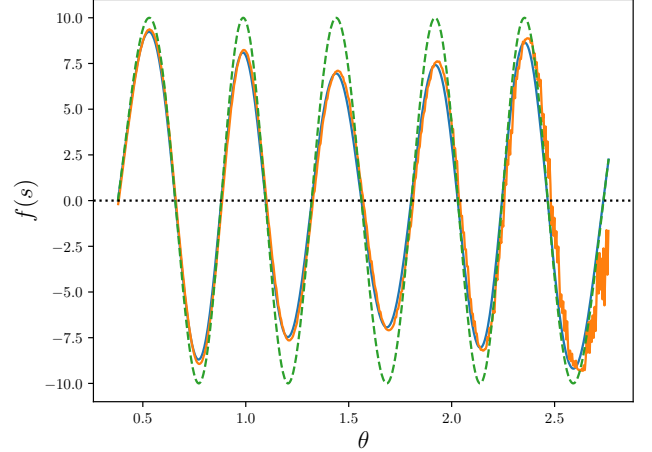


Figure 1. Blue solid curve shows a numerical solution of Equation (10) on a specific field line $p \approx 7.3R_*$ and $\kappa = \omega p / c \approx 12.74$. The numerical solution is obtained using an adaptive Dormand-Prince RK45 algorithm. The orange curve shows an interpolated result from a 2D axisymmetric force-free simulation (Bernardi et al. in prep.), and the dashed green curve shows the reference function $\sin(k_{\parallel}s)$, where $k_{\parallel} = \omega / c$. The interpolated FFE simulation results deteriorates at large θ due to significant dephasing when the wave reaches the opposite footpoint.

Figure 1 shows a numerical solution for Equation (10) on a specific field line, in comparison with the result from a 2D axisymmetric force-free simulation and the reference solution $\sin(k_{\parallel}s)$. One can see that the solution exactly replicates the results from our 2D force-free simulation. The solution is wave-like with the same wavelength $\lambda = 2\pi / k_{\parallel}$, but there is an amplitude modulation that decreases near the equatorial plane compared to $\sin(k_{\parallel}s)$. This amplitude modulation can be interpreted as a correction on the $r^{-3/2}$ amplitude dependence, and is effectively equivalent to the evolution of a WKB mode as $k_{\parallel} \rightarrow \infty$.

Since Equation (10) is a second order equation, it admits two linearly independent solutions. In general, we write these two solutions as f_1 and f_2 , which can be chosen to be the analog of $\cos kx$ and $\sin kx$. The full time-dependent

solution can therefore be constructed as:

$$B_\phi^{(1)}(t) = r^{-3/2}(f_1 + if_2)e^{-i\omega t}. \quad (11)$$

It is understood that the Alfvén wave is the real part of this solution, but the imaginary part is necessary when using Equation (7) to compute the wave electric field. Since f_1 and f_2 are completely determined by solving a relatively simple ODE, this way of constructing the time-dependent solution is computationally much more efficient than evolving a time-dependent PDE, such as done by Bransgrove et al. (2020). A more detailed description of how f_1 and f_2 are obtained is deferred to Appendix B.

3. SECOND ORDER: CONVERSION TO FMS WAVES

Now that we have a solution of the first order normal mode corresponding to general small-amplitude Alfvén waves in dipole geometry, we can evaluate the second order field quantities $\mathbf{B}^{(2)}$, $\mathbf{E}^{(2)}$, and $\mathbf{j}^{(2)}$. This will allow us to study nonlinear wave conversion phenomena directly. In the rest of this paper, we will focus on the spontaneous evolution of a single small-amplitude Alfvén wave, and defer the more complicated case of interaction between different waves to a future study.

3.1. Formalism

Assuming that the solution at first order only contains a single Alfvén wave normal mode described by Equation (4), the second order current has only three terms:

$$\begin{aligned} \mathbf{j}^{(2)} = & \frac{c}{4\pi} \left[\frac{\mathbf{B}^{(0)} \cdot \nabla \times \mathbf{B}^{(2)}}{B_0^2} \mathbf{B}^{(0)} \right. \\ & + \frac{\mathbf{B}^{(0)} \cdot \nabla \times \mathbf{B}^{(1)}}{B_0^2} \mathbf{B}^{(1)} \\ & \left. + \nabla \cdot \mathbf{E}^{(1)} \frac{\mathbf{E}^{(1)} \times \mathbf{B}^{(0)}}{B_0^2} \right]. \end{aligned} \quad (12)$$

The term $\mathbf{B}^{(1)} \cdot \nabla \times \mathbf{B}^{(1)}$ vanishes due to $\nabla \times \mathbf{B}^{(1)}$ being in the $\hat{\boldsymbol{\phi}}$ direction. Similarly $\mathbf{E}^{(1)} \cdot \nabla \times \mathbf{E}^{(1)}$

vanishes due to $\nabla \times \mathbf{E}^{(1)}$ only present in the $\hat{\boldsymbol{\phi}}$ direction. The B^2 term in the denominators expands into $B^2 = B_0^2 + 2\mathbf{B}^{(1)} \cdot \mathbf{B}^{(0)} + 2\mathbf{B}^{(2)} \cdot \mathbf{B}^{(0)} + (\mathbf{B}^{(1)})^2 + \dots$, but since $\mathbf{B}^{(1)} \cdot \mathbf{B}^{(0)} = 0$, the denominator has no first order corrections, therefore the extra terms only come in at $\mathbf{j}^{(3)}$ or above.

The three terms in Equation (12) have well-defined directions. The first term is an Alfvén wave current along the background field, with exactly the same structure as $\mathbf{j}^{(1)}$. It leads to a correction to our first order Alfvén wave solution without changing its polarization, therefore the solution is still fully described by what was discussed in Section 2. The amplitude and frequency of this second order Alfvén wave is apparently unrelated to the first order wave, and need to be determined by additional constraints such as energy conservation.

The second and third terms in Equation (12) are both along the $\hat{\boldsymbol{\phi}}$ direction, so we can group them and denote them as $\mathbf{j}_\phi^{(2)}$. Note that $\mathbf{j}_\phi^{(2)}$ only depends on the first order Alfvén wave solution, therefore it only acts as a source term for the second order wave. The equations for second-order perturbations sourced by this current are:

$$\begin{aligned} \partial_t \mathbf{E}^{(2)} &= c \nabla \times \mathbf{B}^{(2)} - 4\pi \mathbf{j}_\phi^{(2)}, \\ \partial_t \mathbf{B}^{(2)} &= -c \nabla \times \mathbf{E}^{(2)}. \end{aligned} \quad (13)$$

Equations (13) are identical to the vacuum linear Maxwell equations with an external current. The direction of \mathbf{j} suggests that $\mathbf{E}^{(2)}$ is only along the $\hat{\boldsymbol{\phi}}$ direction, and the structure of the equations suggests wave solutions that are degenerate with vacuum electromagnetic waves. Both of these properties point to a fms wave. Therefore, we can interpret the first order Alfvén wave acting as an antenna, producing time-varying $\mathbf{j}_\phi^{(2)}$ that sources a second order fms wave. Since both terms in $\mathbf{j}_\phi^{(2)}$ are second order in $\mathbf{B}^{(1)}$ or $\mathbf{E}^{(1)}$, the oscillation frequency ω_2 of $\mathbf{j}_\phi^{(2)}$ is twice the original Alfvén

wave frequency, $\omega_2 = 2\omega$. The source fms wave is expected to have the same frequency as $\mathbf{j}_\phi^{(2)}$. More quantitative discussion of the frequency structure will be presented in Section 3.2.

In Cartesian geometry, the second and third terms in Equation (12) exactly cancel each other, therefore there is no spontaneous production of second order fms waves. Similarly, under the usual WKB assumption where $kL \gg 1$, the background magnetic field is locally constant and the first order solution behaves like a plane wave, therefore j_ϕ also vanishes. However, in general curvilinear geometry when the curvature radius is not too much larger than the wavelength, there is no guarantee that these two terms cancel. As a result, we argue that when a first order Alfvén wave propagates on curved field lines, it should spontaneously source a second order fms wave by acting as an antenna. The resulting fms wave has double the original Alfvén wave frequency. This is a geometrical nonlinear effect that is not captured in the WKB approximation. In the limit of $kL \gg 1$ however, we do expect the spontaneous conversion to fms waves to become negligible, as the wave solution approaches the usual plane wave solution in a uniform magnetic field.

The analysis in this section differs from existing literature based on 3-wave interaction (see e.g. Lyubarsky 2019; Yuan et al. 2021) in two ways. Firstly, if one attributes the generation of fms waves from the primary Alfvén wave to some form of 3-wave interaction, then the natural question is what is the Alfvén wave interacting with. Yuan et al. (2021) hypothesized that it is the interaction between the primary Alfvén wave and a back-propagating Alfvén wave that produces the outgoing fms wave. However, this picture does not make a definitive prediction about the frequency of the outgoing wave, since there is not much information to constrain the back-propagating Alfvén wave. Secondly, 3-wave interaction typically requires the kine-

matic constraint of $\mathbf{k}' = \mathbf{k}_1 + \mathbf{k}_2$. However, a quasi-isotropic outgoing spherical fms wave would need to involve \mathbf{k}' of all directions, necessitating a wide range of combinations of interacting waves \mathbf{k}_1 and \mathbf{k}_2 that are difficult to extract from the propagating, spatially extended primary Alfvén wave.

The analysis outlined above shows that a primary Alfvén wave spontaneously converting to a second order fms wave is the result of nonlinearity on curved magnetic field lines. This analysis makes a definitive prediction that the frequency of the outgoing fms wave is twice the Alfvén wave frequency, which agrees with the simulations performed by Yuan et al. (2021). This picture also allows us to quantitatively compute the properties of the resulting fms wave using classical electrodynamics. We present such a calculation in Section 3.2.

3.2. Quantitative Calculations

The key to computing the spontaneous conversion of a single Alfvén wave to fms waves is the second order current density $\mathbf{j}_\phi^{(2)}$ in Equation (12). Once we find the Fourier components of $\mathbf{j}_\phi^{(2)}$, we can use it to compute the vector potential $A_\phi^{(2)}$, which can be used to compute the electric and magnetic fields of the fms wave. The Fourier components of the vector potential $A_\phi^{(2)}$ can also be used to directly compute the power and the angular dependence of the outgoing wave.

In component form, the equation for $\mathbf{j}_\phi^{(2)}$ can be written as:

$$\begin{aligned} j_\phi^{(2)} &= \frac{c}{4\pi} \left[\frac{B_\phi^{(1)}}{B_0} \left(\frac{\delta}{\sin^3 \theta} \frac{\partial B_\phi^{(1)}}{\partial p} + \frac{1 - 3 \cos^2 \theta}{r \delta \sin \theta} B_\phi^{(1)} \right) \right. \\ &\quad \left. - \frac{E_p^{(1)}}{B_0} \left(\frac{\delta}{\sin^3 \theta} \frac{\partial E_p^{(1)}}{\partial p} + \frac{4(1 - 3 \cos^4 \theta)}{r \delta^3 \sin \theta} E_p^{(1)} \right) \right] \\ &= \frac{c}{4\pi} \left[\frac{B_\phi^{(1)}}{B_0} \hat{D}_B B_\phi^{(1)} - \frac{E_p^{(1)}}{B_0} \hat{D}_E E_p^{(1)} \right], \end{aligned} \tag{14}$$

where we have introduced two operators \hat{D}_B and \hat{D}_E to facilitate subsequent calculations. As evident from Equation (14), the second order current depends on the partial derivative of the wave fields across field lines, ∂_p . Since the waves on each field line propagate independently, this derivative is determined by the initial phase gradient of the wave perpendicular to the field lines, as well as the phase difference built up due to different field line lengths (Chen et al. 2022a). Therefore, $j_\phi^{(2)}$ is in general nonzero when the Alfvén wave propagates on curved field lines, and the production of a fms wave is inevitable.

Next, we want to find the Fourier components of $j_\phi^{(2)}$. The real part of Equation (11) can be written as:

$$B_\phi^{(1)} = \hat{f}_1 \cos \omega t + \hat{f}_2 \sin \omega t, \quad (15)$$

where $\hat{f}_i = r^{-3/2} f_i$. Plugging this into Equation (14), the structure of the first term is:

$$\begin{aligned} B_\phi^{(1)} \hat{D}_B B_\phi^{(1)} &= \frac{1}{2} \left[\left(\hat{f}_1 \hat{D}_B \hat{f}_2 + \hat{f}_2 \hat{D}_B \hat{f}_1 \right) \sin 2\omega t \right. \\ &\quad + \left(\hat{f}_1 \hat{D}_B \hat{f}_1 - \hat{f}_2 \hat{D}_B \hat{f}_2 \right) \cos 2\omega t \\ &\quad \left. + \left(\hat{f}_1 \hat{D}_B \hat{f}_1 + \hat{f}_2 \hat{D}_B \hat{f}_2 \right) \right]. \end{aligned} \quad (16)$$

The second term in Equation (14) has a similar structure. Therefore, $j_\phi^{(2)}$ consists of an oscillating component with frequency 2ω , as well as a non-oscillating component. The oscillating component sources an outgoing fms wave with frequency 2ω , as discussed in Section 3.1. The non-oscillating component does not directly source an outgoing wave, but as the primary Alfvén wave bounces back and forth on a closed field line tube, this component will lead to oscillations at a frequency comparable to c/L , where L is the length of the field line. This low frequency oscillation may source an additional fms wave, as is seen in simulations performed by Bernardi et al (in prep).

To compute the concrete radiation power in fms waves, we specialize to a particular magnetospheric configuration. In a static, axisymmetric dipole magnetosphere, an Alfvén wave is launched from the surface in a flux tube between p_1 and p_2 . The magnitude of the Alfvén wave is determined by the boundary conditions at launch point (see Appendix B for more discussion). In order for the wave profile to smoothly go to zero at the $p = p_{1,2}$ boundaries, we apply a transverse profile function $a(p) = \cos^2(\pi(p - p_m)/(p_2 - p_1))$, where $p_m = (p_1 + p_2)/2$ marks the approximate middle point of the flux tube.

The Alfvén wave is launched from the magnetic footpoint in the northern hemisphere. For simplicity, the boundary at the southern footpoint of the flux tube is assumed to be perfectly absorbing, which allows us to avoid the discussion of wave reflection. We solve Equation (10) for 100 evenly distributed field lines inside the flux tube $p_1 \leq p \leq p_2$, then interpolate the results to an evenly spaced grid in (r, θ) . The toroidal current $j_\phi^{(2)}$ is computed using a second-order finite difference scheme on the spherical grid. A result of such a calculation is shown in Figure 2.

Once we have computed the spatial dependence of $j_\phi^{(2)}$, we can separate the oscillating part and the constant part in Equation (16). The constant part does not produce an electromagnetic wave since we do not treat the reflection of the primary Alfvén wave. The oscillatory part directly produces the following vector potential (see e.g. Jackson 1999):

$$A_\phi^{(2)}(\mathbf{x}) = \frac{1}{c} \int \frac{j_\phi^{(2)}(\mathbf{x}') e^{ikr}}{r} d^3x', \quad (17)$$

where $r = |\mathbf{x} - \mathbf{x}'|$, $k = \omega_2/c$, and a $e^{-i\omega_2 t}$ time dependence is understood for both j_ϕ and A_ϕ . Then the total power emitted in fms waves can be computed by integrating the outgoing Poynt-

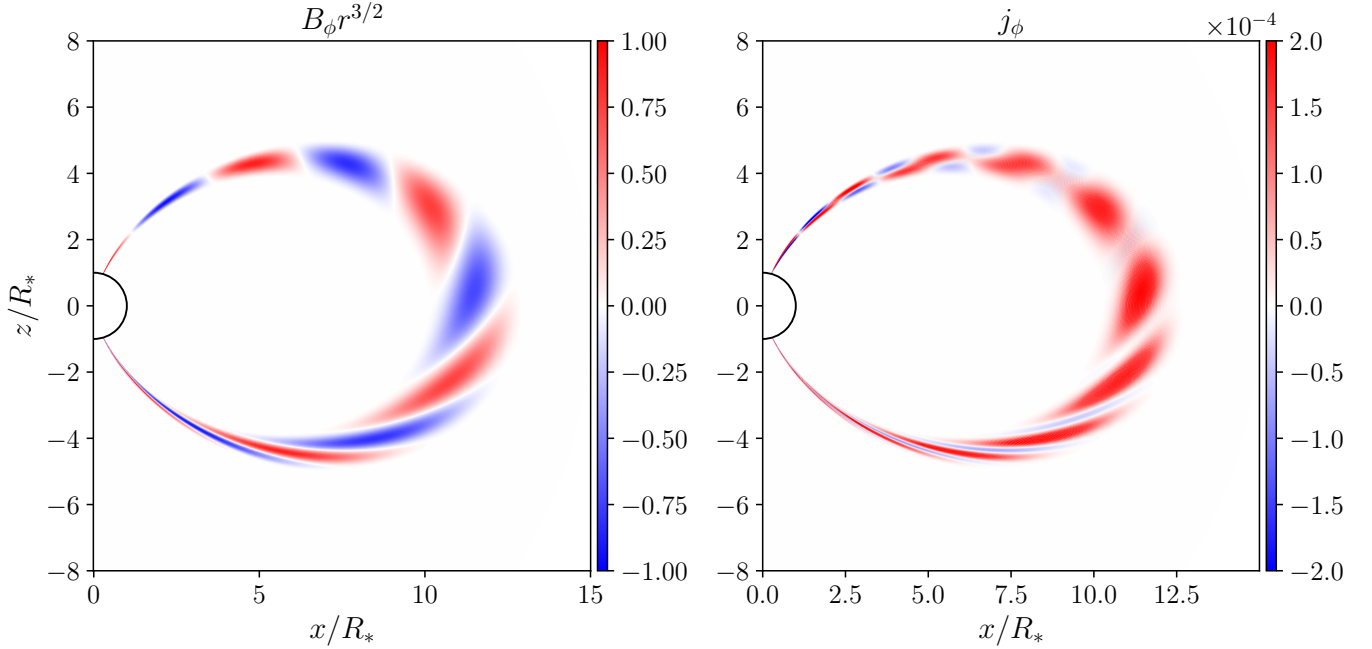


Figure 2. Alfvén wave solution computed using the method described in Section 3.2, evaluated at an arbitrary time $t = 13R_*/c$. The wave amplitude is $\delta B/B_0 \approx 1/40$ at launch point. The wave is launched in the flux tube $10R_* \leq p \leq 13R_*$, with wavelength $\lambda \approx 6R_*$. The solution is interpolated onto a 2000×2000 2D spherical grid.

ing flux at a large radius R :

$$\begin{aligned} L_{\text{fms}} &= \frac{c}{4\pi} \int |\mathbf{E} \times \mathbf{B}| R^2 d\Omega \\ &= \frac{c}{4\pi} \int |\omega A_\phi^{(2)}|^2 R^2 d\Omega. \end{aligned} \quad (18)$$

The square amplitude $|A_\phi^{(2)}|^2$ also gives the angular profile of the outgoing fms wave.

3.3. Scaling

We performed this calculation for a series of different $\delta B/B_0$ and p_m . We keep $p_2 - p_1$ fixed to be $2R_*$, so that the transverse size of the flux tube remains roughly the same. The Alfvén wavelength is taken to be $\lambda_A = R_*$. The luminosity is computed at a very large radius, $r = 400R_*$, far away from the maximum extent of any of the flux tubes considered. The results are shown in Figure 3. The power in the outgoing fms wave scales exactly quadratically with respect to $(\delta B/B_0)_{\text{eq}}$, which is the relative amplitude of the primary Alfvén wave at the

equator. We measure this quantity at the middle of the flux tube, $p_m = (p_1 + p_2)/2$. The fms wave power also scales approximately linearly with p_m , which is proportional to the length of the flux tube.

The quadratic scaling with respect to the relative amplitude of the wave is not a surprise, as $j_\phi^{(2)}$ manifestly depends on $(\delta B^{(1)})^2$. The linear scaling with respect to p_m is likely a result of a larger emitting region size, which scales linearly with p_m . Both of these features agree with what was reported in FFE simulations (Yuan et al. 2021). The full numerical simulations include effects beyond second order, as well as the reflection of the primary Alfvén wave and its self-intersection. However, it was shown that most of the $\omega_2 = 2\omega$ fms wave production happens during the first passing of the Alfvén wave, therefore we expect that the calculation here is a relatively good approximation of the full nonlinear behavior until $(\delta B/B_0)_{\text{eq}} \gg 1$.

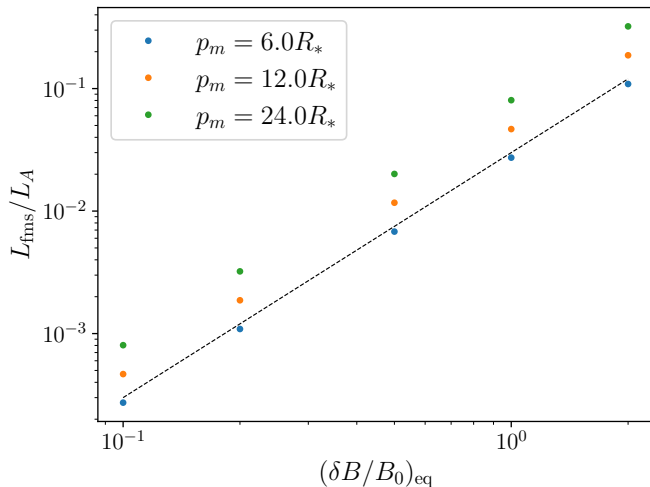


Figure 3. Scaling of the fms wave conversion efficiency with respect to the relative amplitude of the original Alfvén wave measured at the equator. Black dashed line corresponds to $L_{\text{fms}}/L_A \propto (\delta B/B_0)_{\text{eq}}^2$. The conversion efficiency scales quadratically with $(\delta B/B_0)_{\text{eq}}$, and scales linearly with the total flux tube length. When varying p_m , we keep the transverse size of the flux tube $p_2 - p_1$ to be fixed at $2R_*$. The Alfvén wavelength is taken to be $\lambda_A = R_*$.

The reason that outgoing fms wave power significantly reduces after reflection is due to the dephasing of the wave. As the Alfvén wave propagates on the curved flux tube, the path length of the inner edge of the flux tube is shorter than the outer edge. The wave therefore builds up a phase difference on adjacent field lines. This effect can be clearly seen in Figure 2. Since A_ϕ is the integral of j_ϕ with an oscillatory function e^{ikr} , the contribution becomes small when the variation scale of j_ϕ becomes much smaller than $k = \omega/c$. The amount of dephasing is especially significant for extended field lines (Chen et al. 2022a), and we expect the only effective window for wave conversion via this channel is during the initial passing of the Alfvén wave in the flux tube, before significant dephasing has happened.

The same formalism outlined in this section can be applied to multi-wave interactions. It

is well-known that in the force-free limit, $A + A \rightarrow F$ is an allowed nonlinear conversion channel (Thompson & Blaes 1998). In the formalism developed in this paper, one can include this effect by simply considering $B_\phi^{(1)}$ as a sum of multiple wave components, $B_\phi^{(1)} = B_{\phi,a}^{(1)} + B_{\phi,b}^{(1)}$, and calculate the toroidal current using this sum. The resulting current will have oscillating components with frequencies $\omega = \omega_a \pm \omega_b$, $2\omega_a$, and $2\omega_b$, in addition to the bouncing frequency associated with the length of the flux tube. The outgoing fms wave luminosity will scale with the product of the relative amplitudes.

The energy of the outgoing fms wave comes at the expense of the original Alfvén wave. The second order Alfvén component can account for this amplitude decrease. However, full energy conservation including the second order fms wave is difficult to incorporate into the calculation. The energy of the second order fms wave shows up at fourth order in the energy expansion, which is at the same order as terms such as $\mathbf{B}^{(0)} \cdot \mathbf{B}^{(4)}$ or $\mathbf{B}^{(1)} \cdot \mathbf{B}^{(3)}$. Since we terminate the asymptotic expansion at the second order, treating the issue of energy conservation is beyond the scope of this paper.

4. CLOSED ZONE OF A ROTATING MAGNETOSPHERE

In a rotating magnetosphere, the background electric field $\mathbf{E}^{(0)}$ is no longer zero. Instead, $\mathbf{E}^{(0)} = -(\mathbf{v}/c) \times \mathbf{B}^{(0)}$. As a result, the asymptotic expansion discussed in Section 2 needs to be modified. In this section, we focus on the limit of slow rotation, and employ a two-scale asymptotic expansion in both $\delta B/B_0$ and the rotation speed v_ϕ/c . The first expansion is identical to what we used in the previous section, and we continue to use superscript (1) to denote the first order terms. We will use an additional superscript [1] to denote the first order corrections due to the rotation of the star. The rotation-induced background electric field is written as $\mathbf{E}^{(0),[1]}$ in this notation system.

We will focus on the closed zone of the magnetosphere, where no poloidal current is flowing. The open zone in the force-free magnetosphere will have nonzero magnetospheric current flowing to infinity, and a nonzero $B_\phi^{(0),[1]}$ as a result (see e.g. [Contopoulos et al. 1999](#)). For slowly rotating neutron stars such as most magnetars discovered so far, the closed zone dominates the region near the star, therefore the results of this section should apply to most of the Alfvén waves launched from the surface.

Under the two-scale expansion, the (0)-th order current density acquires a second-order correction in v_ϕ/c :

$$\begin{aligned} \mathbf{j}^{(0),[1]} &= 0, \\ \mathbf{j}^{(0),[2]} &= -\frac{c}{4\pi} \nabla \cdot \mathbf{E}^{(0),[1]} \frac{\mathbf{E}^{(0),[1]} \times \mathbf{B}^{(0),[0]}}{B_0^2} \quad (19) \\ &= \rho_{\text{GJ}} v_\phi \hat{\phi}, \end{aligned}$$

where ρ_{GJ} is the Goldreich-Julian charge density ([Goldreich & Julian 1969](#)). The current is second order because both v_ϕ and ρ_{GJ} are first order in rotation. This second order current sources a change in $B^{(0)}$ leading to a deviation from the non-rotating dipole solution in the steady state in the closed zone:

$$\nabla \times \mathbf{B}^{(0),[2]} = 4\pi \mathbf{j}^{(0),[2]}. \quad (20)$$

There is no correction to the background magnetic field at [1]-st order in the closed zone. Therefore, to first order in v_ϕ/c , the magnetic field lines remain dipole-shaped, and we can continue using (q, p, ϕ) as our field-aligned coordinate system.

The non-rotating Alfvén wave solution we obtained in Section 2 is now denoted by $\mathbf{B}^{(1),[0]}$ and $\mathbf{E}^{(1),[0]}$. The equations for the first order Alfvén wave remain unchanged:

$$\begin{aligned} \partial_t \mathbf{B}_A^{(1),[0]} &= -c \nabla \times \mathbf{E}_A^{(1),[0]} \\ \partial_t \mathbf{E}_A^{(1),[0]} &= c \nabla \times \mathbf{B}_A^{(1),[0]} - 4\pi \mathbf{j}^{(1),[0]}, \end{aligned} \quad (21)$$

where $\mathbf{j}^{(1),[0]}$ is given by Equation (5). We are now interested in the nonlinear effects at first

order in rotation, assuming that a single Alfvén wave described by Equation (4) is injected into the magnetosphere.

Since $\mathbf{E}^{(0),[1]} = -(\mathbf{v}/c) \times \mathbf{B}_0 \propto \hat{p}$, under axisymmetry, $\nabla \times \mathbf{E}^{(0),[1]} \sim \partial_q E_p^{(0),[1]} \hat{\phi}$. Similarly we have already established in the previous section that $\nabla \times \mathbf{E}^{(1),[0]} \sim \partial_q E_p^{(1),[0]} \hat{\phi}$. Therefore, both $\mathbf{E}^{(0),[1]} \cdot \nabla \times \mathbf{E}^{(1),[0]}$ and $\mathbf{E}^{(1),[0]} \cdot \nabla \times \mathbf{E}^{(0),[1]}$ are zero. As a result, the nonzero terms in the 1st order correction to $\mathbf{j}^{(1)}$ are:

$$\begin{aligned} \mathbf{j}^{(1),[1]} &= \frac{c}{4\pi} \left[\frac{\mathbf{B}^{(0),[0]} \cdot \nabla \times \mathbf{B}^{(1),[1]}}{B_0^2} \mathbf{B}^{(0),[0]} \right. \\ &\quad - \nabla \cdot \mathbf{E}^{(1),[0]} \frac{\mathbf{E}^{(0),[1]} \times \mathbf{B}^{(0),[0]}}{B_0^2} \quad (22) \\ &\quad \left. - \nabla \cdot \mathbf{E}^{(0),[1]} \frac{\mathbf{E}^{(1),[0]} \times \mathbf{B}^{(0),[0]}}{B_0^2} \right]. \end{aligned}$$

The structure of $\mathbf{j}^{(1),[1]}$ is very similar to the second order current in the non-rotating case, given in Equation (12). The first term is formally identical to the [0]-th order current (5), and represents the current associated with the [1]-st order corrected Alfvén wave that flows along the background field line. The remaining two terms are both along the $\hat{\phi}$ direction, and we group them as $\mathbf{j}_\phi^{(1),[1]}$.

Since $\mathbf{j}_\phi^{(1),[1]}$ does not depend on $\mathbf{E}^{(1),[1]}$ or $\mathbf{B}^{(1),[1]}$, the Maxwell equations for the [1]-st order electric and magnetic fields sourced by this current are identical to the vacuum, linear version:

$$\begin{aligned} \partial_t \mathbf{B}_F^{(1),[1]} &= -c \nabla \times \mathbf{E}_F^{(1),[1]} \\ \partial_t \mathbf{E}_F^{(1),[1]} &= c \nabla \times \mathbf{B}_F^{(1),[1]} - 4\pi \mathbf{j}_\phi^{(1),[1]}. \end{aligned} \quad (23)$$

Therefore, the [1]-st order toroidal current again acts as an antenna that radiates fast waves which is identical to vacuum electromagnetic waves in the FFE limit (albeit with a particular polarization). We added subscript F to \mathbf{E} and \mathbf{B} to distinguish it from the corrections to the Alfvén wave at this order. Since

$\mathbf{j}_\phi^{(1),[1]}$ has only one factor of $\mathbf{E}^{(1),[0]}$, its frequency will be the same as the Alfvén wave frequency, in contrast with the nonrotating case where the fast wave at (2)-nd order has double the Alfvén wave frequency. Its amplitude scales as $O(\delta B/B_0)O(v_\phi/c)$, which is different from the non-rotating case. At very small $\delta B/B_0$, this first order fast wave dominates the Alfvén to fast wave conversion, while at larger amplitudes the second order non-rotating contribution will dominate. This is consistent with the force-free simulations conducted by Yuan et al. (2021).

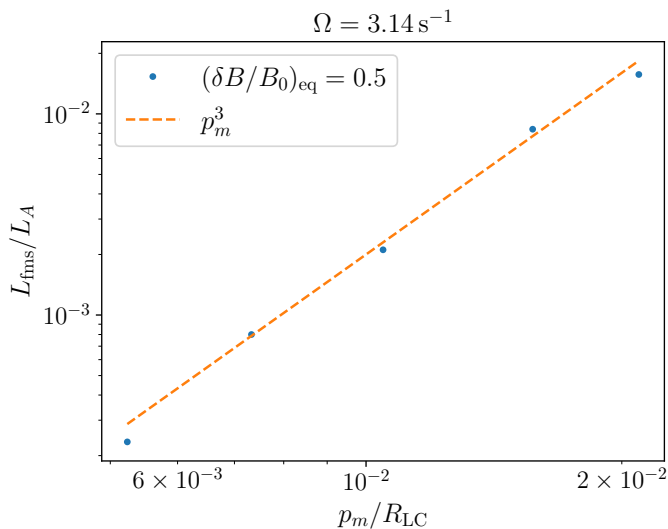


Figure 4. The Alfvén to fms wave conversion efficiency at first order in rotation scales with p_m^3 . The calculations are done with fixed $(\delta B/B_0)_{eq} = 0.5$ and fixed rotation frequency $\Omega = 3.14 \text{ s}^{-1}$, which corresponds to a rotation period of 2s. When calculating the current in different flux tubes, we keep $p_2 - p_1 = 10R_*$ for all cases, so that the transverse size of the flux tube remains roughly the same. The Alfvén wave length is taken to be $5R_*$. L_{fms} is computed at $R = 1000R_*$.

The power of fms waves produced in the rotating magnetosphere can be computed in the same way as described in Section 3.2. Figure 4 shows the scaling of conversion efficiency with respect to the maximum field line extent p_m . The result is consistent with $L_{fms}/L_A \propto p_m^3$.

This is not surprising, as the fms wave amplitude scales as $\delta B v_\phi$, and its luminosity scales as $\delta B^2 v_\phi^2$. Since the primary Alfvén wave luminosity also scales as δB^2 , this factor drops out. On the other hand, $v_\phi = \rho \Omega \sim p_m \Omega$, leading to a scaling factor of p_m^2 . In addition, we expect the fms wave luminosity to scale linearly with the length of the flux tube, similar to the nonrotating case. Therefore $L_{fms}/L_A \propto p_m^3$ is consistent with analysis presented in this section. Due to the rather strong scaling with p_m , we expect L_{fms}/L_A to reach order unity near $p_m/R_{LC} \sim 0.1$. This fraction may be lower if the duration of the Alfvén wave is shorter than the light-crossing time of the flux tube, but it seems relatively easy to convert a significant fraction of the Alfvén wave energy to fms waves in a rotating magnetosphere, as long as the primary Alfvén wave propagates on field lines that extend to a fraction of the light cylinder radius.

Note that our main focus is not to find the corresponding first order normal modes in a rotating magnetosphere. Such a calculation has been carried out by Yuan et al. (2021) in their Appendix D, under a WKB approximation where $kL \gg 1$. In fact, their result includes up to second order terms in rotation, or order (1), [2] in our language: $\delta \mathbf{E} = \mathbf{E}^{(1),[0]} + \mathbf{E}^{(1),[1]} + \mathbf{E}^{(1),[2]}$. Instead, we keep track of the separate orders and only keep the first order corrections in rotation, which leads to much simpler equations for each order without the WKB assumption. In fact, since the [2]-nd order corrections to the background magnetic field is nonzero in the closed zone, it would have been inappropriate if we extended the dipole-based formalism in this paper to second order in rotation.

5. DISCUSSIONS

In this paper, we have solved for the small-amplitude Alfvénic normal modes in a dipole background magnetic field. Using an asymptotic expansion, we demonstrated that a single Alfvén wave will spontaneously convert to

fast magnetosonic waves as it propagates on the curved field line. In a non-rotating dipole magnetosphere, the resulting fms wave will have frequency twice the original Alfvén wave frequency. In the closed zone of a rotating force-free magnetosphere, the fms wave first shows up at first order in a two-scale expansion, and its frequency is the same as the original Alfvén wave frequency. In both cases, the fast wave is sourced by a toroidal electric current that acts like an antenna. This picture not only elucidates the wave conversion process, but also provides a concrete means to compute the properties of the outgoing fms wave using standard electrodynamics techniques, without resorting to global FFE simulations.

The numerical solution of the Alfvén wave profile can be a useful tool in future research on wave phenomena in the magnetospheres of neutron stars, especially for low frequency Alfvén waves whose wavelengths are comparable to the global scales. It can also be used as a benchmark tool for testing FFE or PIC simulation codes in spherical coordinates. Although we do not treat reflection in this paper, it can be added relatively easily using the usual trick of launching additional waves with a time delay from outside the domain. The primary Alfvén wave may interact nonlinearly with its reflection, leading to an enhanced production of fms waves.

This paper mainly concerns the spontaneous evolution of a single Alfvén wave launched from the surface of the neutron star. However, multi-wave interaction (e.g. interaction of the primary Alfvén wave with its reflection) can be included

in the same framework too. In particular, multiple Alfvén waves superimpose linearly at the first order, which will lead to a range of frequency components in the second order current, Equation (14). As a result, fms waves of different frequencies will be sourced, and the calculation is similar to the single wave case.

The fms wave produced from spontaneous conversion may suffer from its own nonlinear effects. For example, if the outgoing fms wave is strong enough, it may steepen within the magnetosphere into a shock at each wavelength (see [Chen et al. 2022b](#); [Beloborodov 2023a](#)). This shock may produce interesting radiation signals such as strong X-ray emission. If the fms wave does not steepen within the magnetosphere, it may interact nonlinearly with the current sheet near the light cylinder, leading to current sheet compression and enhanced reconnection rates (see e.g. [Lyubarsky 2019](#); [Mahlmann et al. 2022](#); [Wang et al. 2023](#)). The results of this paper can provide a framework for estimating the properties of the fms waves converted from Alfvén waves, potentially contributing to a more complete understanding of X-ray or radio bursts from magnetars.

1 We thank Yuanhong Qu and Xinyu Li
 2 for helpful discussions and comments on the
 3 manuscript. AC and YY acknowledge sup-
 4 port from NSF grants DMS-2235457 and AST-
 5 2308111. YY also acknowledges support from
 6 the Multimessenger Plasma Physics Center
 7 (MPPC), NSF grant PHY-2206608, and sup-
 8 port from the Simons Foundation (MP-SCMPS-
 9 00001470).

APPENDIX

A. DIPOLE COORDINATE IDENTITIES

In this appendix we list some common identities in dipole coordinates that are used in the main text. Much of the content here follows [Swisdak \(2006\)](#). First, the dipole coordinates as defined by

equations (1) take the range $q \in (-\infty, \infty)$ and $p \in [0, \infty)$. It is not an orthonormal coordinate system, and the metric tensor is:

$$g_{ij} = \text{diag} \left(\frac{r^6}{\delta^2}, \frac{\sin^6 \theta}{\delta^2}, r^2 \sin^2 \theta \right), \quad (\text{A1})$$

where $\delta = \sqrt{1 + 3 \cos^2 \theta}$. Since Alfvén waves are launched from the stellar surface, it is convenient to define a field line length s that starts at the stellar radius $r = R_*$. This turns out to be nontrivial since the stellar surface does not coincide with a coordinate surface. [Chen et al. \(2022a\)](#) wrote down an exact expression for s for a field line starting at $\mu_0 = \cos \theta_0$:

$$s(p, \mu) = p [F(\mu_0) - F(\mu)], \quad (\text{A2})$$

where $\mu = \cos \theta$ and

$$F(\mu) = \frac{1}{2} \mu \sqrt{1 + 3\mu^2} + \frac{\sinh^{-1}(\sqrt{3}\mu)}{2\sqrt{3}}. \quad (\text{A3})$$

The field line length s can be thought of as a rescaling of the coordinate variable q , although constant s surfaces do not coincide with constant q surfaces. Despite the seemingly complex expression, some of its coordinate derivatives are relatively simple:

$$\frac{\partial s}{\partial q} = \frac{r^3}{\delta}, \quad \frac{\partial s}{\partial \theta} = p \delta \sin \theta. \quad (\text{A4})$$

The 3-dimensional curl of a vector field in these coordinates can be written as:

$$\begin{aligned} \nabla \times \mathbf{A} = & \hat{\mathbf{q}} \left[\frac{\delta}{\sin^3 \theta} \frac{\partial A_\phi}{\partial p} + \frac{1 - 3 \cos^2 \theta}{r \delta \sin \theta} A_\phi - \frac{1}{r \sin \theta} \frac{\partial A_p}{\partial \phi} \right] \\ & + \hat{\mathbf{p}} \left[\frac{1}{r \sin \theta} \frac{\partial A_q}{\partial \phi} - \frac{\delta}{r^3} \frac{\partial A_\phi}{\partial q} + \frac{3 \cos \theta}{r \delta} A_\phi \right] \\ & + \hat{\boldsymbol{\phi}} \left[\frac{\delta}{r^3} \frac{\partial A_p}{\partial q} - \frac{6 \cos \theta}{r \delta^3} (1 + \cos^2 \theta) A_p - \frac{\delta}{\sin^3 \theta} \frac{\partial A_q}{\partial p} - \frac{3 \sin \theta}{r \delta^3} (1 + \cos^2 \theta) A_q \right]. \end{aligned} \quad (\text{A5})$$

The divergence of a 3-dimensional vector field in dipole coordinates is:

$$\begin{aligned} \nabla \cdot \mathbf{A} = & \frac{\delta^2}{r^6} \frac{\partial}{\partial q} \left(\frac{r^3}{\delta} A_q \right) + \frac{\delta^2}{\sin^6 \theta} \frac{\partial}{\partial p} \left(\frac{\sin^3 \theta}{\delta} A_p \right) + \frac{4}{r \delta \sin \theta} A_p + \frac{1}{r \sin \theta} \frac{\partial A_\phi}{\partial \phi} \\ = & \frac{\delta}{r^3} \frac{\partial A_q}{\partial q} - \frac{3 \cos \theta}{r \delta^3} (3 + 5 \cos^2 \theta) A_q + \frac{\delta}{\sin^3 \theta} \frac{\partial A_p}{\partial p} + \frac{4}{r \delta^3 \sin \theta} (1 - 3 \cos^4 \theta) A_p + \frac{1}{r \sin \theta} \frac{\partial A_\phi}{\partial \phi} \end{aligned} \quad (\text{A6})$$

B. ALFVÉN WAVE SOLUTIONS

In this appendix we outline our method to obtain solutions to Equation (10) that represents a propagating wave. This is a second order ODE with no regular singularity points, and its solutions are not described by well-known functions such as hypergeometric functions. We resort to numerical techniques to solve this equation.

In general, a second order linear ODE admits two independent solutions, and the general solution is a linear combination of them:

$$f(\mu) = C_1 f_1(\mu) + C_2 f_2(\mu). \quad (\text{B7})$$

Since we are interested in wave-like solutions, we take the linear combinations $f_1 \pm i f_2$, where the sign corresponds to right-going or left-going waves. We demand the following boundary conditions which mimic $\cos kx$ and $\sin kx$:

$$\begin{aligned} f_1(\mu_0) &= A, & f_1'(\mu_0) &= 0, \\ f_2(\mu_0) &= 0, & f_2'(\mu_0) &= K, \end{aligned} \quad (\text{B8})$$

where A is the overall amplitude of the wave, and K is a constant that needs to be chosen so that f_1 and f_2 are consistent with a traveling wave. We fix the constant by demanding $E_p = -B_\phi$ at the stellar surface, which is equivalent to approximating the solution as a plane wave at the launch point. Although this is an approximation, direct FFE simulations have shown that this assumption is reasonably accurate at the launch point (Bernardi et al. in prep.), but the equality typically ceases hold after the wave has propagated for some distance.

In order to determine K using the condition $E_p = -B_\phi$ at the launch point, we write down the expressions for E_p and B_ϕ using Equation (7) and $\partial s/\partial q = r^3/\delta$:

$$B_\phi = r^{-3/2}(f_1 + i f_2)e^{-i\omega t}, \quad E_p = -\frac{ic}{\omega}r^{-3/2}(\partial_s f_1 + i\partial_s f_2)e^{-i\omega t}. \quad (\text{B9})$$

Therefore, the boundary condition we apply is simply:

$$f_1(s=0) = -\frac{c}{\omega}\partial_s f_2(s=0) \implies K = \frac{\omega p \delta}{c}A. \quad (\text{B10})$$

The resulting solutions f_1 and f_2 are shown in Figure 5. Note that these two solutions are completely determined by the boundary conditions (B8) at the left end, therefore the right boundary conditions are left unconstrained. This choice is to mimic the launching of Alfvén waves from crustal motion at one end. When the wave arrives at the opposite end, it will reflect off the stellar surface, and the full solution will be a linear superposition of the original wave plus an additional incoming wave launched from the opposite footpoint.

REFERENCES

- Beloborodov, A. M. 2022, *PhRvL*, 128, 255003, doi: [10.1103/PhysRevLett.128.255003](https://doi.org/10.1103/PhysRevLett.128.255003)
- . 2023a, *ApJ*, 959, 34, doi: [10.3847/1538-4357/acf659](https://doi.org/10.3847/1538-4357/acf659)
- . 2023b, arXiv e-prints, arXiv:2307.12182, doi: [10.48550/arXiv.2307.12182](https://doi.org/10.48550/arXiv.2307.12182)
- Bransgrove, A., Beloborodov, A. M., & Levin, Y. 2020, *ApJ*, 897, 173, doi: [10.3847/1538-4357/ab93b7](https://doi.org/10.3847/1538-4357/ab93b7)
- Chen, A. Y., Yuan, Y., Beloborodov, A. M., & Li, X. 2022a, *ApJ*, 929, 31, doi: [10.3847/1538-4357/ac59b1](https://doi.org/10.3847/1538-4357/ac59b1)
- Chen, A. Y., Yuan, Y., Li, X., & Mahlmann, J. F. 2022b, arXiv e-prints, arXiv:2210.13506, doi: [10.48550/arXiv.2210.13506](https://doi.org/10.48550/arXiv.2210.13506)
- Contopoulos, I., Kazanas, D., & Fendt, C. 1999, *ApJ*, 511, 351, doi: [10.1086/306652](https://doi.org/10.1086/306652)
- Golbraikh, E., & Lyubarsky, Y. 2023, *ApJ*, 957, 102, doi: [10.3847/1538-4357/acfa78](https://doi.org/10.3847/1538-4357/acfa78)

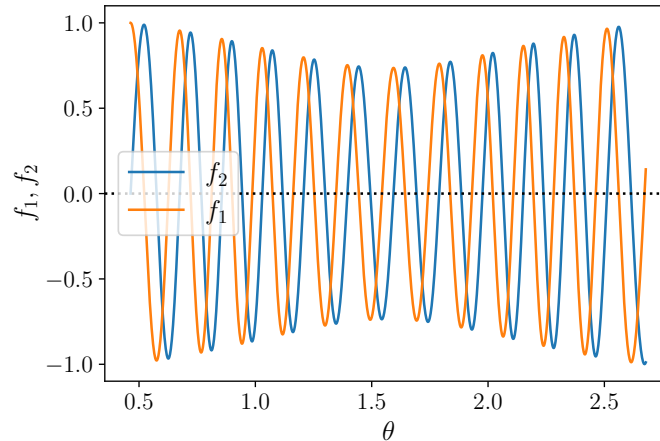


Figure 5. Independent Alfvén wave solutions f_1 and f_2 , normalized such that the maximum amplitude is $A = 1$. The solutions are obtained on the field line $p = 5R_*$, and the wave is launched at frequency $\omega = 2\pi c/R_*$. f_1 is the analog of $\cos kx$ and f_2 is the analog of $\sin kx$.

- Goldreich, P., & Julian, W. H. 1969, *ApJ*, 157, 869, doi: [10.1086/150119](https://doi.org/10.1086/150119)
- Gruzinov, A. 1999, arXiv e-prints, astro, doi: [10.48550/arXiv.astro-ph/9902288](https://doi.org/10.48550/arXiv.astro-ph/9902288)
- Jackson, J. D. 1999, *Classical electrodynamics*, American Association of Physics Teachers
- Kageyama, A., Sugiyama, T., Watanabe, K., & Sato, T. 2006, *Computers and Geosciences*, 32, 265, doi: [10.1016/j.cageo.2005.06.006](https://doi.org/10.1016/j.cageo.2005.06.006)
- Li, X., Beloborodov, A. M., & Sironi, L. 2021, *ApJ*, 915, 101, doi: [10.3847/1538-4357/abfe5f](https://doi.org/10.3847/1538-4357/abfe5f)
- Li, X., Zrake, J., & Beloborodov, A. M. 2019, *ApJ*, 881, 13, doi: [10.3847/1538-4357/ab2a03](https://doi.org/10.3847/1538-4357/ab2a03)
- Lyubarsky, Y. 2019, *MNRAS*, 483, 1731, doi: [10.1093/mnras/sty3233](https://doi.org/10.1093/mnras/sty3233)
- . 2020, *ApJ*, 897, 1, doi: [10.3847/1538-4357/ab97b5](https://doi.org/10.3847/1538-4357/ab97b5)
- Mahlmann, J. F., Philippov, A. A., Levinson, A., Spitkovsky, A., & Hakobyan, H. 2022, *ApJL*, 932, L20, doi: [10.3847/2041-8213/ac7156](https://doi.org/10.3847/2041-8213/ac7156)
- Metzger, B. D., Margalit, B., & Sironi, L. 2019, *MNRAS*, 485, 4091, doi: [10.1093/mnras/stz700](https://doi.org/10.1093/mnras/stz700)
- Nättilä, J., & Beloborodov, A. M. 2022, *PhRvL*, 128, 075101, doi: [10.1103/PhysRevLett.128.075101](https://doi.org/10.1103/PhysRevLett.128.075101)
- Plotnikov, I., & Sironi, L. 2019, *MNRAS*, 485, 3816, doi: [10.1093/mnras/stz640](https://doi.org/10.1093/mnras/stz640)
- Qu, Y., Kumar, P., & Zhang, B. 2022, *MNRAS*, 515, 2020, doi: [10.1093/mnras/stac1910](https://doi.org/10.1093/mnras/stac1910)
- Sironi, L., Plotnikov, I., Nättilä, J., & Beloborodov, A. M. 2021, *PhRvL*, 127, 035101, doi: [10.1103/PhysRevLett.127.035101](https://doi.org/10.1103/PhysRevLett.127.035101)
- Swisdak, M. 2006, arXiv e-prints, physics/0606044, doi: [10.48550/arXiv.physics/0606044](https://doi.org/10.48550/arXiv.physics/0606044)
- TenBarge, J. M., Ripperda, B., Chernoglazov, A., et al. 2021, *Journal of Plasma Physics*, 87, 905870614, doi: [10.1017/S002237782100115X](https://doi.org/10.1017/S002237782100115X)
- Thompson, C., & Blaes, O. 1998, *PhRvD*, 57, 3219, doi: [10.1103/PhysRevD.57.3219](https://doi.org/10.1103/PhysRevD.57.3219)
- Wang, J.-S., Li, X., Dai, Z., & Wu, X. 2023, *Research in Astronomy and Astrophysics*, 23, 035010, doi: [10.1088/1674-4527/acb9de](https://doi.org/10.1088/1674-4527/acb9de)
- Yuan, Y., Beloborodov, A. M., Chen, A. Y., & Levin, Y. 2020, *ApJL*, 900, L21, doi: [10.3847/2041-8213/abafa8](https://doi.org/10.3847/2041-8213/abafa8)
- Yuan, Y., Beloborodov, A. M., Chen, A. Y., et al. 2022, *ApJ*, 933, 174, doi: [10.3847/1538-4357/ac7529](https://doi.org/10.3847/1538-4357/ac7529)
- Yuan, Y., Levin, Y., Bransgrove, A., & Philippov, A. 2021, *ApJ*, 908, 176, doi: [10.3847/1538-4357/abd405](https://doi.org/10.3847/1538-4357/abd405)